

Exactly Solvable Disorder-free Quantum Breakdown Model: Spectrum, Thermodynamics, and Dynamics

Kinya Guan¹ and Hosho Katsura^{1,2,3}

¹*Department of Physics, Graduate School of Science, The University of Tokyo, Tokyo 113-0033, Japan*

²*Institute for Physics of Intelligence, The University of Tokyo, Tokyo 113-0033, Japan*

³*Trans-Scale Quantum Science Institute, The University of Tokyo, Tokyo 113-0033, Japan*

(Dated: March 19, 2026)

We introduce and study a disorder-free version of the quantum breakdown model with all-to-all interactions. The Hamiltonian factorizes into the product of the zero-momentum-mode occupation number and a quadratic Hamiltonian including only pairing terms. This structure makes the model exactly solvable and produces a large set of zero-energy states. We analyze its spectral, thermodynamic, and dynamical properties. In particular, we show how the factorized structure shapes the spectral form factor and the real-time dynamics. We also compute two-point functions and out-of-time-ordered correlators (OTOCs), and find a distinct early-time growth regime in the OTOCs. These results provide a solvable setting in which spectral properties and real-time dynamics can be analyzed in a controlled way in the absence of disorder, spatial structure, and environmental coupling.

I. INTRODUCTION

Non-equilibrium dynamics of quantum many-body systems is one of the central topics in modern condensed-matter physics. A prototypical example is dielectric breakdown in insulators, where a strong electric field drives the system far from equilibrium and induces a sudden onset of conduction. In gases, this process has been studied since the early work of Townsend on ionization avalanches [1], and similar avalanche-like breakdown phenomena have been observed in solids, liquids and chemical reaction networks [2–7]. From a microscopic viewpoint, however, the breakdown process involves highly excited many-body states, strong interactions and, in realistic materials, disorder and coupling to the environment. Because of the enormous Hilbert space and the lack of small parameters, a fully quantum-mechanical description is in general complicated.

Because of this complexity, most previous studies of dielectric breakdown have been formulated at a phenomenological or semi-classical level, in terms of ionization avalanches and discharge plasmas (see, e.g., Refs. [1, 8, 9]). These descriptions capture breakdown fields and macroscopic transport properties, but they do not directly offer a fully quantum many-body picture of the breakdown process.

In strongly correlated electron systems, microscopic quantum descriptions of dielectric breakdown have also been developed, particularly in the context of Mott insulators [10–12]. More recently, an explicitly many-body framework was proposed by Lian, who introduced a *quantum breakdown model* (QBM) on a one-dimensional chain of spinless fermions with a spatially asymmetric interaction intended to mimic the effect of a strong electric field [13–17]. In this model, the interplay between the breakdown interaction, local potentials, and disorder gives rise to a crossover from many-body-localized behavior to quantum-chaotic dynamics, accompanied by Hilbert-space fragmentation and many-body scar states. The QBM therefore provides a concrete setting in which non-equilibrium phenomena associated with dielectric breakdown can be studied within a fully interacting quantum many-body framework.

At the same time, the original QBM already incorpo-

rates several competing ingredients: breakdown interactions, a chemical potential, quenched disorder, and explicit spatial structure along the chain. While this richness makes the model relevant to realistic solid-state situations, it also makes it difficult to identify the specific role played by the breakdown interaction itself. In addition, although certain special Krylov subspaces are analytically tractable, many quantitative properties of the QBM still rely on exact diagonalization of finite chains. It is therefore natural to seek a more minimal and analytically controllable framework that retains the characteristic features of the breakdown mechanism.

In this work, we take a step in this direction by constructing a disorder-free, all-to-all-coupled version of the quantum breakdown model that remains exactly solvable. The interaction is reminiscent of the Sachdev–Ye–Kitaev (SYK) model [18, 19], a canonical example of quantum many-body chaos. This simplified structure allows us to obtain the full energy spectrum and the partition function in closed form, and to analyze thermodynamic quantities as well as real-time correlation functions in a controlled way. In this sense, our model also provides a useful bridge between effective descriptions of dielectric breakdown and analytically tractable many-body models that have been used to probe signatures commonly associated with quantum many-body chaos and scrambling.

In what follows, we use “many-body chaos” in a practical spectral sense, as a universality class captured by random matrix theory (RMT). The motivation for invoking RMT is to focus on properties that are insensitive to microscopic interaction details. In generic interacting systems that thermalize within a fixed symmetry sector, local spectral correlations become universal even though the global density of states remains model dependent [20]. RMT provides a minimal benchmark for these universal correlations, and an RMT-like system is expected to show the characteristic dip–ramp–plateau structure in the spectral form factor (SFF) [21].

On the dynamical side, we probe scrambling through out-of-time-ordered correlators (OTOCs), which directly measure operator growth in real time [22–24]. These two perspectives are related but not equivalent [25]. A standard example where an RMT-like SFF and fast operator growth coexist is the SYK

model with random couplings [18, 19, 21, 23, 24]. However, disorder-free SYK models with uniform couplings provide a nontrivial clean example in which the two diagnostics separate: the SFF does not develop an RMT ramp, while OTOCs still exhibit a distinct early-time rapid-growth window before saturation [26]. This is exactly the situation we want to test in the breakdown setting.

The paper is organized as follows. In Sec. II, we define the disorder-free all-to-all quantum breakdown model and set notation. In Sec. III, we derive the exact solution by reducing the Hamiltonian to a quadratic pairing problem. In Sec. IV, we discuss spectral and static properties, including the exact structure of the spectrum, thermodynamics, and the spectral form factor. In Sec. V, we study real-time dynamics, two-point functions, and out-of-time-ordered correlators.

II. MODEL

We consider N spinless complex fermionic modes c_i, c_i^\dagger ($i = 1, \dots, N$) obeying

$$\{c_i, c_j^\dagger\} = \delta_{ij}, \quad \{c_i, c_j\} = \{c_i^\dagger, c_j^\dagger\} = 0. \quad (1)$$

The disorder-free, fully connected version of the quantum breakdown model is described by the Hamiltonian

$$H = \frac{J}{N} \sum_{i=0}^{N-1} \sum_{0 \leq j < k < l \leq N-1} \left(c_i^\dagger c_j c_k c_l + c_i^\dagger c_k^\dagger c_j^\dagger c_l \right), \quad (2)$$

where J sets the interaction scale. In the following, we take $J = 1$. The overall factor $1/N$ is introduced for convenience. A schematic illustration of the model is shown in Fig. 1.

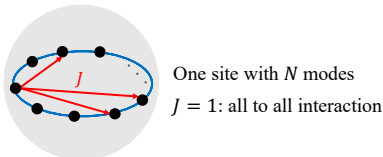


FIG. 1. Schematic illustration of the disorder-free all-to-all quantum breakdown model. A single site contains N fermionic modes, and the interaction couples them uniformly with strength $J = 1$.

Let

$$N_f = \sum_{i=0}^{N-1} c_i^\dagger c_i \quad (3)$$

denote the total fermion number operator. Since the interaction changes particle number by ± 2 , the $U(1)$ symmetry is broken, while fermion parity is conserved:

$$[H, (-1)^{N_f}] = 0. \quad (4)$$

Although the present model is not defined in one dimension, it is convenient to regard the fermionic modes as being

arranged on a one-dimensional ring and introduce the corresponding discrete Fourier modes. In particular, the zero-momentum mode

$$f_0 = \frac{1}{\sqrt{N}} \sum_{i=0}^{N-1} c_i, \quad (5)$$

will play a crucial role in the following analysis. For convenience, we also define the cubic operator

$$Q = \frac{1}{\sqrt{N}} \sum_{0 \leq j < k < l \leq N-1} c_j c_k c_l. \quad (6)$$

The Hamiltonian can then be written as

$$H = f_0^\dagger Q + Q^\dagger f_0. \quad (7)$$

III. EXACT SOLUTION

The exact solution follows from factorizing Q as

$$Q = f_0 A \quad (8)$$

with the fermionic quadratic form

$$A = \frac{1}{2} \sum_{j,k=0}^{N-1} \mathcal{A}_{jk} c_j c_k, \quad \mathcal{A}_{jk} = \begin{cases} +1, & j < k, \\ 0, & j = k, \\ -1, & j > k, \end{cases} \quad (9)$$

which implies

$$H = f_0^\dagger f_0 A + A^\dagger f_0^\dagger f_0. \quad (10)$$

Let $n_0 \equiv f_0^\dagger f_0$. A direct reduction to $H = (A + A^\dagger)n_0$ is obstructed because $[n_0, A] \neq 0$. We resolve this by switching to a Fourier basis and dropping terms that necessarily vanish in (10).

Define Fourier modes on a ring,

$$f_p = \frac{1}{\sqrt{N}} \sum_{j=0}^{N-1} c_j e^{-i\theta_p j}, \quad \theta_p = \frac{2\pi p}{N} \quad (11)$$

with $p = 0, 1, \dots, N-1$, which satisfy

$$\{f_p, f_{p'}^\dagger\} = \delta_{p,p'}, \quad \{f_p, f_{p'}\} = 0. \quad (12)$$

Then A takes the pairing form

$$A = \frac{1}{2} \sum_{p,q} \tilde{\mathcal{A}}_{pq} f_p f_q, \quad \tilde{\mathcal{A}}_{pq} = i \cot\left(\frac{\theta_q}{2}\right) \delta_{p+q,0 \pmod{N}}. \quad (13)$$

See Appendix A for a derivation. Here the key point is that terms containing f_0 drop out of (10) because

$$n_0 f_0 = f_0^\dagger n_0 = 0. \quad (14)$$

We therefore define \tilde{A} by discarding all contributions with $p = 0$ or $q = 0$,

$$\tilde{A} \equiv \frac{1}{2} \sum_{p,q=1}^{N-1} \tilde{\mathcal{A}}_{pq} f_p f_q, \quad (15)$$

which satisfies $[n_0, \tilde{A}] = 0$. As a result,

$$H \equiv H_{\text{pair}} n_0, \quad (16)$$

where

$$H_{\text{pair}} = \tilde{A} + \tilde{A}^\dagger = \frac{i}{2} \sum_{q=1}^{N-1} \cot\left(\frac{\theta_q}{2}\right) \left(f_{N-q} f_q - f_q^\dagger f_{N-q}^\dagger\right). \quad (17)$$

The pairing Hamiltonian H_{pair} can be diagonalized by a Bogoliubov transformation. For each independent pair $(q, N-q)$ with $q = 1, \dots, \lfloor (N-1)/2 \rfloor$, we introduce the complex fermions

$$\gamma_{q\sigma} = \frac{1}{\sqrt{2}} \left(f_q - i\sigma f_{N-q}^\dagger\right), \quad \sigma = \pm 1, \quad (18)$$

which satisfy

$$\{\gamma_{q\sigma}, \gamma_{p\tau}^\dagger\} = \delta_{qp} \delta_{\sigma\tau}. \quad (19)$$

In terms of these operators,

$$H_{\text{pair}} = \sum_{q=1}^{\lfloor (N-1)/2 \rfloor} \sum_{\sigma=\pm 1} \sigma \epsilon_q n_{q\sigma}, \quad (20)$$

where $n_{q\sigma} \equiv \gamma_{q\sigma}^\dagger \gamma_{q\sigma}$ and $\epsilon_q \equiv \cot(\theta_q/2)$. Here, $\lfloor \cdot \rfloor$ denotes the floor function. For even N , there is also an unpaired mode at $q = N/2$. Since $\epsilon_{N/2} = 0$, its occupation does not change the energy.

Combining (16) and (20), the full Hamiltonian factorizes as

$$H = \left(\sum_{q=1}^{\lfloor (N-1)/2 \rfloor} \sum_{\sigma=\pm 1} \sigma \epsilon_q n_{q\sigma} \right) n_0, \quad (21)$$

which is the starting point for the exact evaluation of the spectrum, the SFF, thermodynamics, and real-time correlation functions. Since $n_0 \in \{0, 1\}$, the Hilbert space splits into two sectors. In what follows, we refer to the $n_0 = 0$ sector as the *frozen sector* and the $n_0 = 1$ sector as the *active sector*.

IV. SPECTRUM AND STATIC PROPERTIES

This section discusses the spectral and thermodynamic properties that follow from the factorized Hamiltonian in Eq. (21). We first describe the exact spectral structure and the degeneracy at zero energy, then turn to the spectral form factor, and finally derive the partition function and thermodynamics.

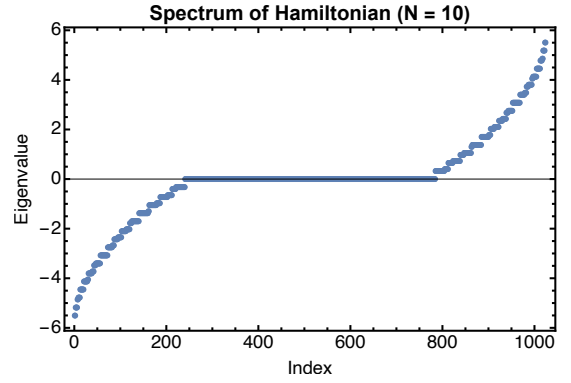


FIG. 2. Spectrum for $N = 10$. The extensive zero-energy plateau receives contributions from both the frozen and active sectors, while the nonzero spectrum arises from the active sector.

A. Spectral structure

A key feature of the spectrum is the extensive degeneracy at zero energy. Equation (21) shows that the spectrum separates according to the eigenvalue of n_0 .

Let $D_0(N)$ denote the number of zero-energy states for a given system size N . In the frozen sector ($n_0 = 0$), the energy vanishes identically, so this sector contributes 2^{N-1} zero-energy states. In the active sector ($n_0 = 1$), the many-body energies are

$$E = \sum_{q=1}^{\lfloor (N-1)/2 \rfloor} \sum_{\sigma=\pm 1} \sigma \epsilon_q n_{q\sigma}. \quad (22)$$

Additional zero-energy states arise when $n_{q+} = n_{q-}$ for all q . Combining these with the frozen-sector contribution, we obtain the lower bound on $D_0(N)$:

$$\underline{D}_0(N) = \begin{cases} 2^{N-1} + 2^{(N-1)/2}, & N \text{ odd,} \\ 2^{N-1} + 2^{N/2}, & N \text{ even.} \end{cases} \quad (23)$$

For even N , the second term includes an extra factor of 2 coming from the unpaired zero-energy mode at $q = N/2$.

Figure 2 shows a representative spectrum (here $N = 10$), illustrating the broad zero-energy plateau and the nonzero spectrum arising from the active sector. Table I compares the numerical values of $D_0(N)$ with Eq. (23), showing that the bound is saturated for all N except for $N = 14$. We note in passing that a similar extensive degeneracy at zero energy has been reported in the disorder-free complex SYK model [27].

Finally, we estimate the bandwidth W of the nonzero spectrum in the active sector. From Eq. (22), with $n_{q\sigma} \in \{0, 1\}$, the maximum energy is obtained by setting $n_{q,+} = 1$ and $n_{q,-} = 0$ for all q , while the minimum is obtained by the opposite choice. Therefore,

$$E_{\text{max}} = \sum_{q=1}^{\lfloor (N-1)/2 \rfloor} \epsilon_q, \quad E_{\text{min}} = -E_{\text{max}}, \quad (24)$$

N	4	5	6	7	8	9	10	11	12	13	14
$D_0(N)$	12	20	40	72	144	272	544	1056	2112	4160	8324
$\underline{D}_0(N)$	12	20	40	72	144	272	544	1056	2112	4160	8320

TABLE I. Exact numbers of zero-energy states, $D_0(N)$, and the corresponding lower bounds, $\underline{D}_0(N)$, for different system sizes N . The discrepancy at $N = 14$ arises from an accidental finite-size cancellation among the values of $\cot(\pi q/N)$, which generates additional zero eigenvalues not accounted for by the generic formula.

so that

$$W \equiv E_{\max} - E_{\min} = 2 \sum_{q=1}^{\lfloor (N-1)/2 \rfloor} \cot\left(\frac{\pi q}{N}\right). \quad (25)$$

For even N , the unpaired mode at $q = N/2$ has zero energy and does not affect the bandwidth. As shown in Appendix B, $W = O(N \log N)$ at large N .

B. Spectral form factor

We characterize spectral correlations using the spectral form factor (SFF), defined by

$$g(t, \beta) = \left| \frac{\text{Tr} e^{(it-\beta)H}}{\text{Tr} e^{-\beta H}} \right|^2 = \left| \frac{Z(\beta - it)}{Z(\beta)} \right|^2, \quad (26)$$

where

$$Z(\beta) \equiv \text{Tr} e^{-\beta H} \quad (27)$$

is the partition function. In systems with random-matrix-like level correlations, the SFF typically exhibits dip–ramp–plateau behavior [21].

In the present model, $Z(\beta)$ is available in closed form, so the SFF can be evaluated exactly. We first consider the infinite-temperature case $\beta = 0$. Figure 3 shows $g(t, 0)$ for representative system sizes. The solid lines are numerical results, while the dashed lines show the small- t expansion

$$g(t, 0) = 1 - \frac{t^2}{4N} \binom{N}{3} + \frac{t^4}{24} \frac{1}{4N} \left[\frac{7}{2N} \binom{N}{3}^2 + 8 \binom{N}{5} \right] + O(t^6), \quad (28)$$

which captures the initial decay. At later times, the SFF decays from $g(0, 0) = 1$ and rapidly approaches a plateau at $1/4$, without developing a clear linear ramp. This plateau originates from the exponentially large number of zero-energy states discussed in Sec. IV A, which contributes a strictly time-independent term to $Z(-it)$ at $\beta = 0$, while the other states dephase. Consequently, $Z(-it)/Z(0) \rightarrow 1/2$ at late times, giving $g(t, 0) \rightarrow 1/4$.

At finite temperature, the SFF shows oscillatory revivals rather than a clear ramp, as shown in Fig. 4. This is qualitatively similar to the behavior found in other integrable models, such as the clean transverse-field Ising chain [28]. In the

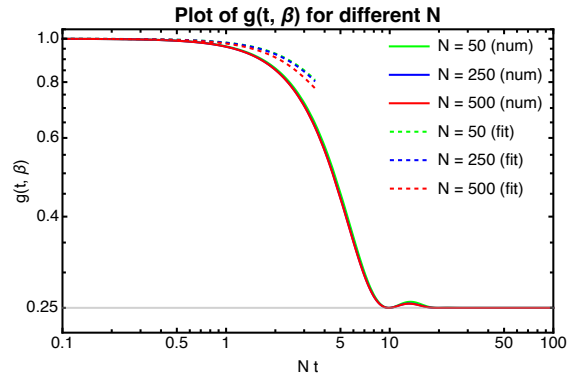


FIG. 3. Infinite-temperature SFF $g(t, 0)$ for several system sizes N . Solid lines show the numerical results, while dashed lines show the small- t expansion in Eq. (28).

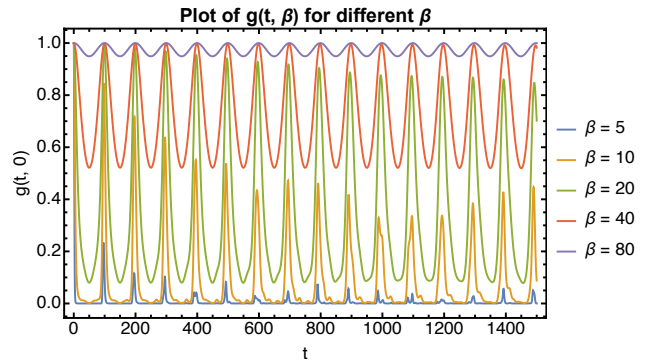


FIG. 4. Finite-temperature SFF $g(t, \beta)$ for $N = 50$ at several β . The behavior shows oscillatory revivals rather than a clear ramp, and the revival peaks can vary irregularly in height.

present model, however, the revival peaks can vary irregularly in height, which is clearly visible, for example, at $\beta = 10$.

The derivation of Eq. (28), together with the large- N analysis of the approach to the plateau, is given in Appendix C.

C. Partition function and thermodynamics

We now derive the partition function, which has already appeared in the SFF through Eq. (26). As discussed earlier, in the frozen ($n_0 = 0$) sector, the Hamiltonian vanishes, so the contribution to $Z(\beta)$ is purely entropic. In the active ($n_0 = 1$) sector, the Hamiltonian is a sum of independent modes with energies $\pm \epsilon_q$. As a result, the partition function can be written in closed form as

$$\begin{aligned} Z(\beta) &= 4^{\lfloor (N-1)/2 \rfloor} + \prod_{q=1}^{\lfloor (N-1)/2 \rfloor} \left(1 + e^{+\beta \epsilon_q} \right) \left(1 + e^{-\beta \epsilon_q} \right) \\ &= 4^{\lfloor (N-1)/2 \rfloor} + \prod_{q=1}^{\lfloor (N-1)/2 \rfloor} 4 \cosh^2 \left(\frac{\beta \epsilon_q}{2} \right). \end{aligned} \quad (29)$$

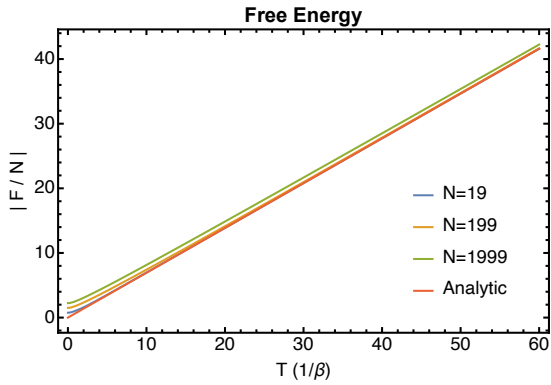


FIG. 5. Free energy density $|F(T)|/N$ as a function of $T = 1/\beta$ in the high-temperature regime. The numerical data (computed for $N = 19, 199, 1999$) approach the analytic line $T \log 2$ for large T .

For even N , the unpaired $q = N/2$ mode contributes an overall factor of 2 regardless of β , which we absorb into the normalization constant since it cancels out in normalized quantities such as the SFF.

From $Z(\beta)$, we obtain the free energy $F(T) = -\beta^{-1} \log Z(\beta)$ and the entropy $S(T) = -\partial F/\partial T$, where $T = 1/\beta$. For finite systems, the N -dependence of these quantities will be made explicit when needed.

Two limits are particularly transparent: the high- and low-temperature limits. In the high-temperature limit $\beta \rightarrow 0$, Eq. (29) gives $Z(\beta) \rightarrow 2 \cdot 4^{(N-1)/2}$, hence

$$\frac{F(T)}{N} \rightarrow -T \log 2, \quad \frac{S(T)}{N} \rightarrow \log 2, \quad (30)$$

up to $O(1/N)$ corrections. Figure 5 compares the numerical free energy with the asymptotic line $|F(T)|/N = T \log 2$.

At low temperature, we take the thermodynamic limit $N \rightarrow \infty$ at fixed β first and then consider $\beta \rightarrow \infty$. In this order of limits, the active sector dominates, and the leading behavior is

$$\frac{F(T, N)}{N} = -\frac{1}{\pi} (\log N + \gamma - \log \pi) - \frac{\pi}{6} T^2 + O(T^4), \quad (31)$$

where γ is the Euler–Mascheroni constant. The first term represents the zero-temperature contribution in this order of limits. Its slow $\log N$ dependence is nonuniversal and originates from the small- q tail $\epsilon_q = \cot(\pi q/N) \sim N/(\pi q)$, which makes the sum over single-particle energies scale as $N \log N$ (Appendix B). This logarithmic growth is a consequence of the present normalization, where no Kac-type rescaling is introduced [29, 30]. The corresponding entropy density is

$$\frac{S(T, N)}{N} = \frac{\pi}{3} T + O(T^3). \quad (32)$$

The temperature-dependent correction $-(\pi/6)T^2$ in Eq. (31) and the linear-in- T entropy are controlled by modes near $\theta = \pi$ where $\epsilon(\theta) = \cot(\theta/2)$ vanishes and can be linearized. This reproduces the standard low-temperature scaling of 1 + 1-dimensional systems with linear low-energy dispersion, and

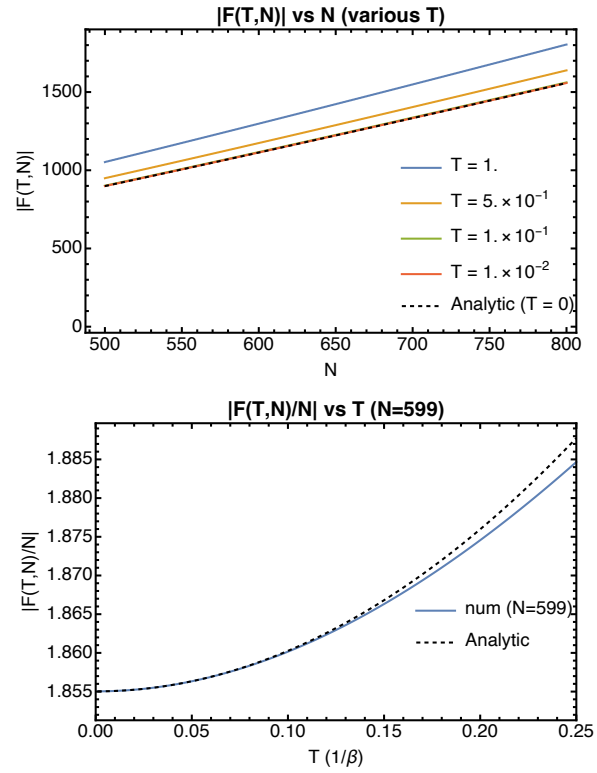


FIG. 6. Free energy in the low-temperature regime. Upper panel: free energy $|F(T, N)|$ as a function of N for several temperatures, approaching the asymptotic form $\frac{N}{\pi} (\log N + \gamma - \log \pi)$ shown by the dashed line. Lower panel: free energy density $|F(T, N)/N|$ as a function of $T = 1/\beta$ at fixed $N = 599$. The solid lines show numerical results, and the dashed line shows the analytical prediction in Eq. (31).

matches the usual CFT form at the level of the leading temperature dependence [31–33]. Figure 6 compares these asymptotic forms with numerical results. The derivation uses cotangent-sum asymptotics and a standard Fermi–Dirac integral, which we collect in Appendix B.

V. DYNAMICS AND CORRELATIONS

The factorized form of the Hamiltonian in Eq. (16) greatly simplifies the analysis of the real-time dynamics in a particularly transparent way. Introducing the projectors onto the two sectors distinguished by the eigenvalues of n_0 ,

$$P_0 \equiv 1 - n_0, \quad P_1 \equiv n_0, \quad (33)$$

the full evolution separates into a static contribution from the frozen sector and a nontrivial contribution generated by the quadratic pairing Hamiltonian H_{pair} in the active sector. The exact projector form of the time-evolution operator and its consequences for operator evolution are given in Appendix D.

We consider thermal expectation values $\langle \dots \rangle = \text{Tr}[\rho(\beta) \dots]$ with $\rho(\beta) = e^{-\beta H}/Z(\beta)$, where $Z(\beta)$ is the partition function defined in Eq. (27). The sector structure

of $e^{-\beta H}$ implies that the thermal expectation value of any observable admits a decomposition into contributions from individual sectors. We define

$$\langle \mathcal{O} \rangle^\alpha \equiv \frac{\text{Tr}(P_\alpha e^{-\beta H} \mathcal{O})}{\text{Tr}(P_\alpha e^{-\beta H})}, \quad \alpha = 0, 1, \quad (34)$$

together with the corresponding sector weights

$$w_\alpha(\beta, N) \equiv \frac{\text{Tr}(P_\alpha e^{-\beta H})}{Z(\beta)}, \quad w_0 + w_1 = 1. \quad (35)$$

Then

$$\langle \mathcal{O} \rangle = w_0 \langle \mathcal{O} \rangle^0 + w_1 \langle \mathcal{O} \rangle^1. \quad (36)$$

In particular, the sector weight $w_1(\beta, N)$ is

$$w_1(\beta, N) = \frac{Z_{\text{pair}}(\beta)}{4^{\lfloor (N-1)/2 \rfloor} + Z_{\text{pair}}(\beta)}, \quad (37)$$

where

$$Z_{\text{pair}}(\beta) = \prod_{q=1}^{\lfloor (N-1)/2 \rfloor} (1 + e^{+\beta \epsilon_q})(1 + e^{-\beta \epsilon_q}), \quad (38)$$

is the active-sector partition function, see Eq. (D6). In each sector, the density matrix is Gaussian. In the frozen sector, it reduces to an infinite-temperature ensemble of the $(N-1)$ nonzero-momentum modes, whereas in the active sector it is determined by the quadratic Hamiltonian H_{pair} . Wick's theorem therefore applies within each sector separately, and all real-time correlators can be reduced to the corresponding Green functions. The details of the Wick reduction and the extension of the correlators to complex time are given in Appendix D.

A. Two-point functions

We study the real-time finite-temperature Green functions

$$(G_{XY})_{jk}(t) \equiv \langle X_j(t) Y_k(0) \rangle, \quad X, Y \in \{c, c^\dagger\}, \quad (39)$$

and their momentum-space counterparts in the Fourier basis f_p defined in Eq. (11). Let $(G_{XY}^\alpha)_{jk}(t)$ denote the corresponding sector-resolved correlator $\langle X_j(t) Y_k(0) \rangle^\alpha$ for $\alpha = 0, 1$. Then Eq. (36) gives

$$(G_{XY})_{jk}(t) = w_0 (G_{XY}^0)_{jk}(t) + w_1 (G_{XY}^1)_{jk}(t). \quad (40)$$

In the frozen sector the Hamiltonian vanishes, so all correlators are time-independent and coincide with the infinite-temperature contractions on the nonzero-momentum modes. All nontrivial time dependence comes from the active sector and is governed by H_{pair} in Eq. (17).

Within the active sector, H_{pair} decouples into independent Bogoliubov pairs $(q, N-q)$. For $q \neq 0$ (and $q \neq N/2$ when

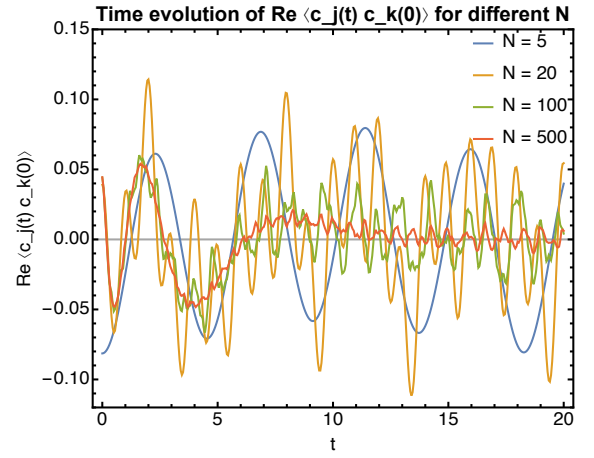


FIG. 7. Time evolution of $\text{Re}\langle c_j(t)c_k(0) \rangle$ for $j = 5$ and $k = 1$ at fixed inverse temperature $\beta = 1$, shown for several system sizes N .

N is even) one finds

$$\langle f_q^\dagger(t) f_q(0) \rangle^1 = \frac{1}{2} \left[\cos(\epsilon_q t) - i \tanh\left(\frac{\beta \epsilon_q}{2}\right) \sin(\epsilon_q t) \right], \quad (41)$$

$$\langle f_q(t) f_{N-q}(0) \rangle^1 = -\frac{1}{2} \left[\sin(\epsilon_q t) + i \tanh\left(\frac{\beta \epsilon_q}{2}\right) \cos(\epsilon_q t) \right], \quad (42)$$

with $\epsilon_q = \cot(\theta_q/2)$. The remaining components follow from Hermitian conjugation and fermionic antisymmetry and are given in Appendix D.

Fourier transforming back to real space yields compact expressions for the correlators in terms of mode sums. For example, the anomalous correlator becomes

$$\begin{aligned} \langle c_j(t) c_k(0) \rangle &= i \frac{w_1}{2N} \sum_{q=1}^{\lfloor (N-1)/2 \rfloor} \sin[\theta_q(j-k)] \\ &\times \left[-\sin(\epsilon_q t) - i \tanh\left(\frac{\beta \epsilon_q}{2}\right) \cos(\epsilon_q t) \right]. \end{aligned} \quad (43)$$

The corresponding expressions for $\langle c_j^\dagger(t) c_k^\dagger(0) \rangle$, $\langle c_j(t) c_k^\dagger(0) \rangle$, and $\langle c_j^\dagger(t) c_k(0) \rangle$, are given in Appendix D4; see Eqs. (D18), (D19), and (D20). Equation (43) is a weighted superposition over the active sector frequencies, so increasing N densifies the spectrum ϵ_q , which enhances dephasing. This is consistent with the smoothing trend in Fig. 7.

In the large- N limit, Eq. (43) is replaced by the integral representation

$$\begin{aligned} \langle c_j(t) c_k(0) \rangle &\xrightarrow{N \rightarrow \infty} i \frac{w_1}{2\pi} \int_0^\pi d\theta \sin[\theta(j-k)] \\ &\times \left[-\sin(\epsilon(\theta)t) - i \tanh\left(\frac{\beta \epsilon(\theta)}{2}\right) \cos(\epsilon(\theta)t) \right], \end{aligned} \quad (44)$$

where $\epsilon(\theta) = \cot(\theta/2)$. The large- N expressions for the other correlators are given in Appendix D6. Figure 8 shows

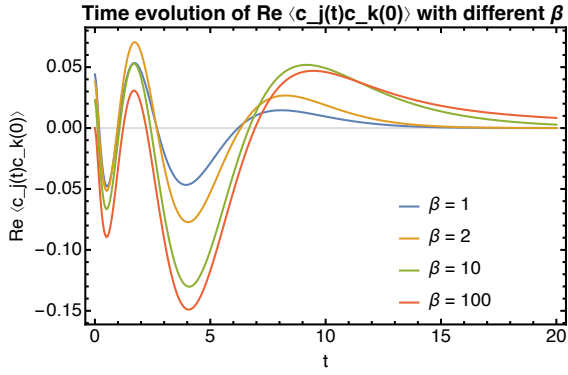


FIG. 8. Time evolution of $\text{Re}\langle c_j(t)c_k(0) \rangle$ in the large- N limit for $j = 5$ and $k = 1$, shown for several inverse temperatures β .

$\text{Re}\langle c_j(t)c_k(0) \rangle$ in the large- N limit for $j = 5$, $k = 1$, and several inverse temperatures β . The correlator first exhibits oscillatory behavior and then approaches a small-amplitude tail on a timescale of order $t_d \sim 10$ – 12 . We use this as a representative dissipation timescale in the sense of Ref. [23].

B. Regularized OTOC

We study an out-of-time-ordered correlator (OTOC) built from local fermion operators. We use the standard regularization with $\rho(\beta)^{1/4}$ insertions [22–25, 34]. We define

$$\begin{aligned} \mathcal{F}(t; \beta) &= \frac{1}{N^2} \sum_{j,m=0}^{N-1} \text{Tr} \left[\rho^{\frac{1}{4}} c_j^\dagger(t) \rho^{\frac{1}{4}} c_m(0) \rho^{\frac{1}{4}} c_j(t) \rho^{\frac{1}{4}} c_m(0) \right], \end{aligned} \quad (45)$$

where the argument β of $\rho(\beta)$ is omitted for brevity. By cyclicity of the trace, this regularization is equivalent to a thermal four-point function with complex time arguments,

$$\begin{aligned} \mathcal{F}(t_1, t_2, t_3, t_4; \beta) &= \frac{1}{N^2} \sum_{j,m=0}^{N-1} \text{Tr} \left[\rho c_j^\dagger(t_1) c_m(t_2) c_j(t_3) c_m(t_4) \right], \end{aligned} \quad (46)$$

evaluated at

$$(t_1, t_2, t_3, t_4) = (t - i\beta/4, 0, t + i\beta/4, i\beta/2), \quad (47)$$

where $\mathcal{F}(t; \beta) \equiv \mathcal{F}(t_1, t_2, t_3, t_4; \beta)$. The steps relating Eqs. (45) and (46) are given in Appendix D.

The sector decomposition of the thermal state implies a corresponding decomposition of the OTOC,

$$\mathcal{F}(t; \beta) = w_0 \mathcal{F}^0(t; \beta) + w_1 \mathcal{F}^1(t; \beta), \quad (48)$$

where \mathcal{F}^0 (\mathcal{F}^1) denotes the OTOC evaluated within the frozen (active) sector. In the frozen sector, the Hamiltonian vanishes, so $\mathcal{F}^0(t; \beta)$ is strictly time independent and enters only through

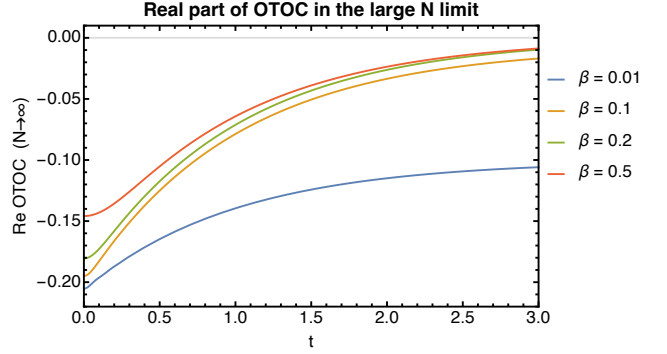


FIG. 9. Real part of the OTOC in the large- N limit. $\text{Re}\mathcal{F}(t; \beta)$ for several inverse temperatures β , showing an early-time increase followed by saturation to the plateau value $-\frac{1}{4} w_0$.

the weight $w_0(\beta, N)$. All nontrivial time dependence comes from $\mathcal{F}^1(t; \beta)$ generated by H_{pair} . The Wick reduction of \mathcal{F}^α is given in Appendix D.

In the large- N limit, the corresponding integral representation is given in Appendix D 6; see Eq. (D33). Figure 9 shows $\text{Re}\mathcal{F}(t; \beta)$ for several inverse temperatures β . For all β , the OTOC starts from a negative value, increases at early times, and then approaches a plateau. Since the time-dependent contribution from the active sector dephases at long times while the frozen sector remains static, the plateau is consistent with

$$\mathcal{F}(t \rightarrow \infty; \beta) = -\frac{1}{4} w_0. \quad (49)$$

At smaller β , this value approaches $-1/4$ as $w_0 \rightarrow 1/2$. The early-time increase in Fig. 9 motivates the exponential fit discussed in Sec. V C.

The sector structure also explains why the SFF and the OTOC capture different aspects of the model. At $\beta = 0$, the SFF is strongly influenced by the extensive degeneracy at zero energy, especially the frozen sector, which contributes a time-independent piece to $\text{Tr} e^{iHt}$ and fixes an $O(1)$ plateau after normalization. By contrast, the time dependence of the OTOC comes entirely from the active sector governed by H_{pair} , while the frozen sector enters only through its thermal weight.

A related coexistence of nonrandom-matrix spectral behavior and a short-time growth window in OTOCs has also been reported in the disorder-free SYK models [26], which provide a useful point of reference for the present solvable model.

C. Early-time exponential fit

To characterize the early-time growth window, we fit $\text{Re}\mathcal{F}(t; \beta)$ to

$$\text{Re}\mathcal{F}(t; \beta) \simeq A e^{\lambda t} + B, \quad (50)$$

where A , B and λ are fitting parameters. The fit is performed in the interval $t \in [0.1\beta, 0.3\beta]$, which is the same window used in Fig. 10 and Table II. Within this window, the numerical data are well described by Eq. (50), and we use λ as an effective

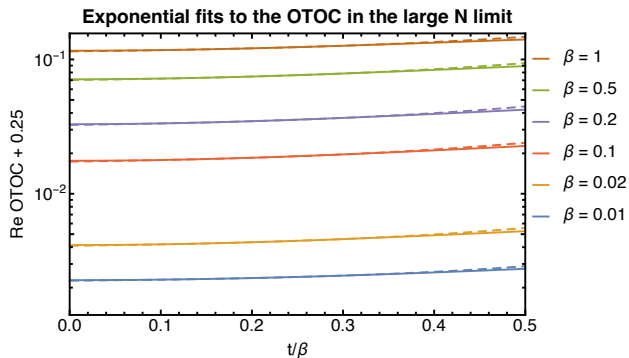


FIG. 10. Exponential fits of the large- N OTOC. Log plot of $\text{Re}\mathcal{F}(t; \beta) + \frac{1}{4}$ as a function of t/β ; solid lines are the numerical data and dashed lines are best-fit curves in the window $t \in [0.1\beta, 0.3\beta]$.

TABLE II. Best-fit parameters of the early-time exponential form in Eq. (50) for different inverse temperatures β . The fits are performed in the window $t \in [0.1\beta, 0.3\beta]$; R^2 denotes the coefficient of determination.

β	A	λ	B	R^2
0.01	0.000066	4.72691	-0.247813	1.000
0.02	0.000184	4.38900	-0.246088	1.000
0.1	0.000860	4.32695	-0.233502	1.000
0.2	0.001605	4.29660	-0.219091	1.000
0.5	0.003302	4.20520	-0.183039	1.000
1	0.004929	4.06101	-0.140081	1.000

short-time growth rate. We do not interpret λ as a Lyapunov exponent [23–25]. In the standard discussion of exponential OTOC growth, the regime associated with a Lyapunov exponent lies well after the dissipation time t_d and well before the scrambling time t_* . In the present model, the two-point function in Fig. 8 suggests a representative dissipation timescale $t_d \sim 10$ – 12 , which is much longer than the fitting window used in Eq. (50). We therefore regard λ only as an effective short-time growth rate.

VI. CONCLUSION AND DISCUSSION

We have constructed a disorder-free all-to-all quantum breakdown model that is exactly solvable and admits closed-form analysis of its spectrum, thermodynamics, and real-time correlators. The key structural feature is the factorization of the Hamiltonian through the zero-momentum-mode occupation $n_0 = f_0^\dagger f_0$, which produces a large set of zero-energy states and separates the dynamics into a frozen sector and an active sector governed by the pairing Hamiltonian H_{pair} .

This structure clarifies why the spectral form factor and the OTOC probe different aspects of the model. The spectral form factor is strongly influenced by the extensive zero-energy degeneracy associated with the frozen sector, and therefore does not develop a clear ramp. By contrast, the OTOC receives its nontrivial time dependence from the active sector and exhibits

an early-time growth regime before approaching a plateau. In this sense, the present model provides a simple solvable example in which spectral and dynamical diagnostics do not track each other in the same way. This is reminiscent of what has been observed in disorder-free SYK-type models [26], although the microscopic structure here is considerably simpler and is directly motivated by breakdown-type interactions.

It is also useful to compare this sector picture with the original QBM. There, special modes and reference configurations restrict the allowed breakdown processes and thereby lead to fragmentation and constrained breakdown dynamics [13–17]. From this viewpoint, the label n_0 plays a similar conceptual role in the present model. In both cases, simple sector information determines whether a given part of the Hilbert space is frozen or supports nontrivial dynamics. The analogy is not exact, because the present model has no explicit spatial structure, but it still offers a useful perspective on the original QBM, especially beyond analytically tractable subsectors.

This interpretation becomes even clearer in a disorder-free version of the one-dimensional breakdown interaction. For uniform couplings, the same Fourier-transform step used here isolates a distinguished mode on each site, analogous to f_0 . This gives a direct interpretation of the resulting Hilbert-space fragmentation; see Appendix E. The present all-to-all model can therefore be viewed as a minimal solvable model that isolates the breakdown-type interaction and shows explicitly how sector structure alone can produce markedly different spectral and dynamical behavior.

These observations suggest natural future directions. One direction is to keep the model disorder-free but increase the interaction complexity, for example by coupling several clean breakdown- or SYK-like blocks into a chain, in order to test when a more pronounced ramp emerges and whether the early-time OTOC growth persists over a broader time range. Another direction is to study random all-to-all breakdown-type interactions, closer in spirit to the original SYK model, and to compare their spectral and dynamical properties with the solvable case studied here. Such comparisons may help clarify more generally how breakdown-type interactions manifest themselves in nonequilibrium quantum dynamics.

ACKNOWLEDGMENTS

We would like to thank Kohei Kawabata for drawing our attention to the quantum breakdown model, and Hironobu Yoshida for helpful discussions. K.G. was supported by Forefront Physics and Mathematics Program to Drive Transformation (FoPM), a World-leading Innovative Graduate Study (WINGS) Program, the University of Tokyo. H.K. was supported by JSPS KAKENHI Grants No. JP23K25783 and No. JP23K25790, and MEXT KAKENHI Grant-in-Aid for Transformative Research Areas A “Extreme Universe” (KAKENHI Grant No. JP21H05191).

Appendix A: Algebraic details of the exact solution

1. Factorization $Q = f_0 A$

Starting from the definitions in the main text, we have

$$\begin{aligned} f_0 A &= \frac{1}{\sqrt{N}} \sum_i c_i \sum_{j < k} c_j c_k \\ &= \frac{1}{\sqrt{N}} \left(\sum_{i < j < k} + \sum_{j < i < k} + \sum_{j < k < i} \right) c_i c_j c_k \\ &= \frac{1}{\sqrt{N}} \sum_{0 \leq i < j < k \leq N-1} c_i c_j c_k = Q, \end{aligned} \quad (\text{A1})$$

which is Eq. (8).

2. Fourier transform of \mathcal{A}_{jk}

Here we derive the Fourier-transformed pairing kernel $\tilde{\mathcal{A}}_{pq}$ appearing in Eq. (13). Define

$$\tilde{\mathcal{A}}_{pq} = \frac{1}{N} \sum_{j,k=0}^{N-1} \mathcal{A}_{jk} e^{i\theta_p j} e^{i\theta_q k}, \quad \theta_p = \frac{2\pi p}{N}, \quad (\text{A2})$$

where $\mathcal{A}_{jk} = +1$ for $j < k$, -1 for $j > k$, and 0 for $j = k$.

It is convenient to use $z \equiv e^{i2\pi/N}$ so that $e^{i\theta_p j} = z^{pj}$. For fixed j , the k -sum splits into $k > j$ and $k < j$ parts:

$$\begin{aligned} \sum_{k=0}^{N-1} \mathcal{A}_{jk} z^{qk} &= \sum_{k=j+1}^{N-1} z^{qk} - \sum_{k=0}^{j-1} z^{qk} \\ &= \frac{z^{q(j+1)}(1 - z^{q(N-j-1)})}{1 - z^q} - \frac{1 - z^{qj}}{1 - z^q}. \end{aligned} \quad (\text{A3})$$

Multiplying by z^{pj} and summing over j gives

$$\begin{aligned} \tilde{\mathcal{A}}_{pq} &= \frac{1}{N} \sum_{j=0}^{N-1} z^{pj} \left[\frac{z^{q(j+1)}(1 - z^{q(N-j-1)})}{1 - z^q} - \frac{1 - z^{qj}}{1 - z^q} \right] \\ &= \frac{1}{N} \sum_{j=0}^{N-1} z^{pj} \frac{z^{q(j+1)} - z^{qj} - z^{qN} + 1}{1 - z^q} \\ &= \frac{1}{N} \sum_{j=0}^{N-1} z^{pj} \frac{(z^q - 1)(z^{qj} + 1)}{1 - z^q} \quad (\text{using } z^{qN} = 1) \\ &= \frac{1 + z^q}{1 - z^q} \frac{1}{N} \sum_{j=0}^{N-1} z^{j(p+q)}. \end{aligned} \quad (\text{A4})$$

The remaining geometric sum enforces momentum conservation:

$$\frac{1}{N} \sum_{j=0}^{N-1} z^{j(p+q)} = \delta_{p+q, 0 \pmod{N}}. \quad (\text{A5})$$

Finally,

$$\frac{1 + z^q}{1 - z^q} = \frac{1 + e^{i\theta_q}}{1 - e^{i\theta_q}} = i \cot\left(\frac{\theta_q}{2}\right), \quad (\text{A6})$$

so we obtain

$$\tilde{\mathcal{A}}_{pq} = i \cot\left(\frac{\theta_q}{2}\right) \delta_{p+q, 0 \pmod{N}}, \quad (\text{A7})$$

which is Eq. (13).

3. Zero-momentum-mode occupation and the commutators

In the main text we replace A by \tilde{A} defined in Eq. (15) by discarding all contributions with $p = 0$ or $q = 0$. Here we justify this step.

First, note that the zero-momentum-mode occupation $n_0 = f_0^\dagger f_0$ satisfies

$$n_0 f_0 = f_0^\dagger n_0 = 0, \quad (\text{A8})$$

so any term in A containing f_0 drops out of $n_0 A$ and $A^\dagger n_0$ in Eq. (10). Equivalently, using $[n_0, f_p] = -\delta_{p,0} f_0$ one finds

$$[n_0, A] = -\frac{1}{2} \sum_{p,q} \tilde{\mathcal{A}}_{pq} (\delta_{p,0} f_0 f_q + \delta_{q,0} f_p f_0), \quad (\text{A9})$$

so $[n_0, A]$ arises only from terms containing the zero mode f_0 . Dropping all contributions with $p = 0$ or $q = 0$ therefore yields

$$[n_0, \tilde{A}] = 0, \quad (\text{A10})$$

and the Hamiltonian becomes

$$H = n_0 \tilde{A} + \tilde{A}^\dagger n_0 = n_0 (\tilde{A} + \tilde{A}^\dagger) \equiv H_{\text{pair}} n_0, \quad (\text{A11})$$

which is Eq. (16) in the main text.

4. Bogoliubov diagonalization of H_{pair}

To diagonalize Eq. (17), we use that $\tilde{\mathcal{A}}_{pq} \propto \delta_{p+q,0}$, so H_{pair} couples only modes $(q, N-q)$. For $q \neq 0$ and, when N is even, $q \neq N/2$, define $\epsilon_q = \cot(\theta_q/2)$ and write

$$\begin{aligned} H_{\text{pair}} &= \frac{i}{2} \sum_{q=1}^{N-1} \epsilon_q \left(f_{N-q} f_q + f_{N-q}^\dagger f_q^\dagger \right) \\ &= i \sum_{q=1}^{\lfloor (N-1)/2 \rfloor} \epsilon_q \left(f_{N-q} f_q - f_q^\dagger f_{N-q}^\dagger \right), \end{aligned} \quad (\text{A12})$$

where we paired q with $N-q$ and used $\epsilon_{N-q} = -\epsilon_q$.

Introduce the Nambu spinor $\Psi_q = (f_q, f_{N-q}^\dagger)^T$ to obtain a 2×2 pairing Hamiltonian for each q ,

$$H_{\text{pair}} = \sum_{q=1}^{\lfloor (N-1)/2 \rfloor} \Psi_q^\dagger \begin{pmatrix} 0 & -i\epsilon_q \\ i\epsilon_q & 0 \end{pmatrix} \Psi_q. \quad (\text{A13})$$

This is diagonalized by the Bogoliubov modes

$$\gamma_{q\sigma} = \frac{1}{\sqrt{2}} \left(f_q - i\sigma f_{N-q}^\dagger \right), \quad \sigma = \pm 1, \quad (\text{A14})$$

which satisfy $\{\gamma_{q\sigma}, \gamma_{p\tau}^\dagger\} = \delta_{qp} \delta_{\sigma\tau}$ and yield

$$H_{\text{pair}} = \sum_{q=1}^{\lfloor (N-1)/2 \rfloor} \sum_{\sigma=\pm 1} \sigma \epsilon_q n_{q\sigma}, \quad n_{q\sigma} = \gamma_{q\sigma}^\dagger \gamma_{q\sigma}, \quad (\text{A15})$$

which is Eq. (20). (We use the normal-ordered form, so possible constant shifts are absorbed into the definition of zero energy, consistent with the extensive exact $E = 0$ sector.)

5. Even- N unpaired mode and Hilbert-space dimension

When N is even, the mode $q = N/2$ is unpaired and $\epsilon_{N/2} = \cot(\pi/2) = 0$. It contributes only a twofold degeneracy independent of energy and temperature. For odd N , the active sector contains $(N-1)/2$ independent pairs and thus $N-1$ Bogoliubov modes; together with n_0 the total Hilbert-space dimension is $2 \times 2^{N-1} = 2^N$. For even N , the active sector contains $N/2 - 1$ independent pairs giving $N-2$ Bogoliubov modes, and the unpaired $q = N/2$ mode contributes an additional factor 2, so the total dimension is again $2 \times 2^{N-2} \times 2 = 2^N$.

Appendix B: Cotangent-sum identities and asymptotics

1. Asymptotics of the cotangent sum

Here we derive the large- N asymptotics of the bandwidth discussed in the main text. Recall that

$$W = 2 \sum_{q=1}^{\lfloor \frac{N-1}{2} \rfloor} \cot\left(\frac{\pi q}{N}\right), \quad (\text{B1})$$

so it suffices to evaluate

$$S_N := \sum_{q=1}^{\lfloor \frac{N-1}{2} \rfloor} \cot\left(\frac{\pi q}{N}\right) \quad (\text{B2})$$

for large N .

We decompose

$$\cot x = \frac{1}{x} + \left(\cot x - \frac{1}{x} \right), \quad (\text{B3})$$

and set $x_q = \pi q/N$. This yields

$$S_N = \frac{N}{\pi} \sum_{q=1}^M \frac{1}{q} + \sum_{q=1}^M \left(\cot x_q - \frac{1}{x_q} \right), \quad M = \left\lfloor \frac{N-1}{2} \right\rfloor. \quad (\text{B4})$$

The first term is expressed using the harmonic number $H_M = \sum_{q=1}^M 1/q$:

$$\frac{N}{\pi} \sum_{q=1}^M \frac{1}{q} = \frac{N}{\pi} H_M = \frac{N}{\pi} (\ln M + \gamma + O(1/M)), \quad (\text{B5})$$

and since $M \sim N/2$ this becomes

$$\frac{N}{\pi} H_M = \frac{N}{\pi} (\ln N + \gamma - \ln 2) + O(1). \quad (\text{B6})$$

The second term is regular at $x = 0$ because $\cot x - 1/x = O(x)$, so it can be approximated by a Riemann sum:

$$\sum_{q=1}^M \left(\cot x_q - \frac{1}{x_q} \right) = \frac{N}{\pi} \int_0^{\pi/2} \left(\cot x - \frac{1}{x} \right) dx + O(1). \quad (\text{B7})$$

Using

$$\int_\varepsilon^{\pi/2} \cot x dx = [\ln \sin x]_\varepsilon^{\pi/2}, \quad \int_\varepsilon^{\pi/2} \frac{dx}{x} = [\ln x]_\varepsilon^{\pi/2}, \quad (\text{B8})$$

and taking $\varepsilon \rightarrow 0^+$ gives

$$\int_0^{\pi/2} \left(\cot x - \frac{1}{x} \right) dx = \ln \frac{2}{\pi}. \quad (\text{B9})$$

Therefore,

$$\begin{aligned} S_N &= \frac{N}{\pi} (\ln N + \gamma - \ln 2) + \frac{N}{\pi} \ln \frac{2}{\pi} + O(1) \\ &= \frac{N}{\pi} (\ln N + \gamma - \ln \pi) + O(1), \end{aligned} \quad (\text{B10})$$

and hence

$$W = 2S_N = \frac{2N}{\pi} (\ln N + \gamma - \ln \pi) + O(1). \quad (\text{B11})$$

2. Low-temperature expansion of the free energy

Here we derive the low-temperature expansion quoted in Eq. (31). Let

$$M := \left\lfloor \frac{N-1}{2} \right\rfloor. \quad (\text{B12})$$

For simplicity we first discuss odd N . For even N , the unpaired mode $q = N/2$ contributes only an overall factor 2 to the partition function and does not affect the temperature-dependent terms.

Starting from Eq. (29), we rewrite the active sector contribution as

$$\prod_{q=1}^M 4 \cosh^2 \left(\frac{\beta \epsilon_q}{2} \right) = \exp \left(\beta \sum_{q=1}^M \epsilon_q \right) \prod_{q=1}^M (1 + e^{-\beta \epsilon_q})^2, \quad (\text{B13})$$

where we used $4 \cosh^2(x/2) = e^x (1 + e^{-x})^2$.

The frozen contribution in Eq. (29) is

$$4^M = \exp(N \log 2 + O(1)). \quad (\text{B14})$$

By Eq. (B10),

$$\sum_{q=1}^M \epsilon_q = \frac{N}{\pi} (\log N + \gamma - \log \pi) + O(1). \quad (\text{B15})$$

Thus, at fixed $\beta > 0$ and large N , the active sector dominates over the frozen sector, and

$$\log Z(\beta) = \beta \sum_{q=1}^M \epsilon_q + 2 \sum_{q=1}^M \log(1 + e^{-\beta \epsilon_q}) + o(N). \quad (\text{B16})$$

Therefore,

$$\frac{F(T, N)}{N} = -\frac{1}{N} \sum_{q=1}^M \epsilon_q - \frac{2}{\beta N} \sum_{q=1}^M \log(1 + e^{-\beta \epsilon_q}) + o(1). \quad (\text{B17})$$

The first term is fixed by Eq. (B15). For the second term, the low-temperature contribution comes from modes near $\theta = \pi$, where $\epsilon_q = \cot(\theta_q/2)$ is small. Writing $q = N/2 - m$, we obtain

$$\epsilon_{N/2-m} = \cot\left(\frac{\pi}{N} \left(\frac{N}{2} - m\right)\right) = \tan\left(\frac{\pi m}{N}\right) = \frac{\pi m}{N} + O\left(\frac{m^3}{N^3}\right). \quad (\text{B18})$$

Taking $N \rightarrow \infty$ first at fixed β , we find

$$\begin{aligned} \lim_{N \rightarrow \infty} \frac{1}{N} \sum_{q=1}^M \log(1 + e^{-\beta \epsilon_q}) &= \lim_{N \rightarrow \infty} \frac{1}{N} \sum_{m=1}^{\infty} \log(1 + e^{-(\beta \pi/N)m}) \\ &= \frac{1}{\pi} \int_0^{\infty} du \log(1 + e^{-\beta u}). \end{aligned} \quad (\text{B19})$$

After rescaling $v = \beta u$,

$$\frac{1}{\pi} \int_0^{\infty} du \log(1 + e^{-\beta u}) = \frac{1}{\beta \pi} \int_0^{\infty} dv \log(1 + e^{-v}). \quad (\text{B20})$$

Using the standard integral

$$\int_0^{\infty} dv \log(1 + e^{-v}) = \frac{\pi^2}{12}, \quad (\text{B21})$$

we obtain

$$\lim_{N \rightarrow \infty} \frac{1}{N} \sum_{q=1}^M \log(1 + e^{-\beta \epsilon_q}) = \frac{\pi}{12} \frac{1}{\beta} + O(\beta^{-3}). \quad (\text{B22})$$

Substituting Eqs. (B15) and (B22) into Eq. (B17), we obtain

$$\frac{F(\beta, N)}{N} = -\frac{1}{\pi} (\log N + \gamma - \log \pi) - \frac{\pi}{6} T^2 + O(T^4), \quad (\text{B23})$$

and hence

$$\frac{S}{N} = -\frac{\partial}{\partial T} \frac{F}{N} = \frac{\pi}{3} T + O(T^3). \quad (\text{B24})$$

This is the result quoted in Sec. IV C.

3. Sum formula for products of \cot^2

In this subsection we derive the identity

$$\sum_{\{q_{i<}\}} \prod_{m=1}^j \cot^2\left(\frac{\pi q_{i_m}}{N}\right) = \frac{1}{N} \binom{N}{2j+1}, \quad (\text{B25})$$

where $\sum_{\{q_{i<}\}}$ denotes the sum over all strictly ordered j -tuples satisfying

$$1 \leq q_{i_1} < q_{i_2} < \dots < q_{i_j} \leq M, \quad M = \left\lfloor \frac{N-1}{2} \right\rfloor. \quad (\text{B26})$$

We first consider odd $N = 2n + 1$. Then $M = n$, and Eq. (B25) becomes

$$\sum_{\{q_{i<}\}} \prod_{m=1}^j \cot^2\left(\frac{\pi q_{i_m}}{2n+1}\right) = \frac{1}{2n+1} \binom{2n+1}{2j+1}. \quad (\text{B27})$$

Here the summation runs over $1 \leq q_{i_1} < \dots < q_{i_j} \leq n$.

Let

$$\theta_q = \frac{\pi q}{2n+1}, \quad q = 1, \dots, n. \quad (\text{B28})$$

From

$$e^{i(2n+1)\theta_q} = (\cos \theta_q + i \sin \theta_q)^{2n+1}, \quad (\text{B29})$$

the imaginary part gives

$$0 = \sum_{k=0}^n (-1)^{n-k} \binom{2n+1}{2k} (\cos \theta_q)^{2k} (\sin \theta_q)^{2(n-k)+1}. \quad (\text{B30})$$

Dividing by $\sin^{2n+1} \theta_q$, we obtain

$$0 = \sum_{k=0}^n (-1)^{n-k} \binom{2n+1}{2k} (\cot \theta_q)^{2k}. \quad (\text{B31})$$

Thus $(\cot \theta_q)^2$ are roots of the polynomial

$$f(x) = \sum_{k=0}^n (-1)^{n-k} \binom{2n+1}{2k} x^k. \quad (\text{B32})$$

Since the coefficient of x^n is $2n+1$, we can write

$$f(x) = (2n+1) \prod_{q=1}^n [x - (\cot \theta_q)^2]. \quad (\text{B33})$$

Comparing the coefficients of x^{n-j} yields Eq. (B27).

For even $N = 2(n+1)$, we have $M = n$, and Eq. (B25) becomes

$$\sum_{\{q_{i<}\}} \prod_{m=1}^j \cot^2\left(\frac{\pi q_{i_m}}{2(n+1)}\right) = \frac{1}{2(n+1)} \binom{2(n+1)}{2j+1}. \quad (\text{B34})$$

Here the summation runs over $1 \leq q_{i_1} < \dots < q_{i_j} \leq n$.

Let

$$\theta_q = \frac{\pi q}{2(n+1)}, \quad q = 1, \dots, n. \quad (\text{B35})$$

Taking the imaginary part of

$$e^{i2(n+1)\theta_q} = (\cos \theta_q + i \sin \theta_q)^{2(n+1)} \quad (\text{B36})$$

gives

$$0 = \sum_{k=0}^n (-1)^{n-k} \binom{2(n+1)}{2k+1} (\cot \theta_q)^{2k}. \quad (\text{B37})$$

The same coefficient comparison yields Eq. (B34), and therefore Eq. (B25).

Appendix C: Technical details for the spectral form factor

1. Small- t expansion at infinite temperature

Here we derive the small- t expansion of the infinite-temperature SFF. At $\beta = 0$,

$$\text{Tr} e^{iHt} = \text{Tr} \mathbb{I} - \frac{t^2}{2} \text{Tr} H^2 + \frac{t^4}{24} \text{Tr} H^4 + O(t^6), \quad (\text{C1})$$

and all odd moments vanish because the spectrum is symmetric under $H \rightarrow -H$.

We present the derivation for odd N . For even N , the unpaired mode $q = N/2$ contributes only an overall factor of 2, independent of t , which cancels in the normalized SFF.

Using

$$H = H_{\text{pair}} n_0, \quad n_0^2 = n_0, \quad [H_{\text{pair}}, n_0] = 0, \quad (\text{C2})$$

we have

$$H^m = (H_{\text{pair}})^m n_0, \quad m \geq 1. \quad (\text{C3})$$

Tracing over $n_0 \in \{0, 1\}$ then gives

$$\text{Tr} H^m = \text{Tr}_{\text{pair}} \left(H_{\text{pair}}^m \right), \quad m \geq 1, \quad (\text{C4})$$

while

$$\text{Tr} \mathbb{I} = 2^N. \quad (\text{C5})$$

Let $M = \lfloor \frac{N-1}{2} \rfloor$, then

$$H_{\text{pair}} = \sum_{q=1}^M \epsilon_q (n_{q+} - n_{q-}), \quad \epsilon_q = \cot\left(\frac{\pi q}{N}\right). \quad (\text{C6})$$

Since different q pairs are independent, for fixed q one has

$$\begin{aligned} \sum_{n_{q+}, n_{q-}} (n_{q+} - n_{q-}) &= 0, \\ \sum_{n_{q+}, n_{q-}} (n_{q+} - n_{q-})^2 &= 2, \\ \sum_{n_{q+}, n_{q-}} (n_{q+} - n_{q-})^4 &= 2, \end{aligned} \quad (\text{C7})$$

where the sum runs over $(n_{q+}, n_{q-}) \in \{0, 1\}^2$.

For the second moment, all cross terms with $q \neq r$ vanish after tracing, so

$$\begin{aligned} \text{Tr}_{\text{pair}} \left(H_{\text{pair}}^2 \right) &= \sum_{q=1}^M \epsilon_q^2 \left(\sum_{n_{q+}, n_{q-}} (n_{q+} - n_{q-})^2 \right) \prod_{r \neq q} \left(\sum_{n_{r+}, n_{r-}} 1 \right) \\ &= \sum_{q=1}^M \epsilon_q^2 (2) 4^{M-1} = 2^{2M-1} \sum_{q=1}^M \epsilon_q^2. \end{aligned} \quad (\text{C8})$$

Using Appendix B, Eq. (B25) with $j = 1$, we obtain

$$\sum_{q=1}^M \epsilon_q^2 = \sum_{q=1}^M \cot^2\left(\frac{\pi q}{N}\right) = \frac{1}{N} \binom{N}{3}, \quad (\text{C9})$$

and hence

$$\text{Tr}_{\text{pair}} \left(H_{\text{pair}}^2 \right) = 2^{2M-1} \frac{1}{N} \binom{N}{3}. \quad (\text{C10})$$

For the fourth moment, only terms with either four powers of the same mode or two powers each of two different modes survive. This gives

$$\begin{aligned} \text{Tr}_{\text{pair}} \left(H_{\text{pair}}^4 \right) &= 2^{2M-1} \left[\sum_{q=1}^M \epsilon_q^4 + 6 \sum_{1 \leq q < r \leq M} \epsilon_q^2 \epsilon_r^2 \right] \\ &= 2^{2M-1} \left[\left(\sum_{q=1}^M \epsilon_q^2 \right)^2 + 4 \sum_{1 \leq q < r \leq M} \epsilon_q^2 \epsilon_r^2 \right]. \end{aligned} \quad (\text{C11})$$

Again using Eq. (B25), now with $j = 2$,

$$\sum_{1 \leq q < r \leq M} \epsilon_q^2 \epsilon_r^2 = \frac{1}{N} \binom{N}{5}, \quad (\text{C12})$$

together with $\sum_q \epsilon_q^2 = \frac{1}{N} \binom{N}{3}$, we find

$$\text{Tr}_{\text{pair}} \left(H_{\text{pair}}^4 \right) = 2^{2M-1} \left[\frac{1}{N^2} \binom{N}{3}^2 + \frac{4}{N} \binom{N}{5} \right]. \quad (\text{C13})$$

Using

$$g(t, 0) = \left| \frac{\text{Tr} e^{iHt}}{2^N} \right|^2, \quad (\text{C14})$$

and substituting Eqs. (C4), (C10), and (C13), we obtain

$$g(t, 0) = 1 - \frac{t^2}{4N} \binom{N}{3} + \frac{t^4}{24} \frac{1}{4N} \left[\frac{7}{2N} \binom{N}{3}^2 + 8 \binom{N}{5} \right] + O(t^6). \quad (\text{C15})$$

2. Exact representation and the plateau

The plateau of the infinite-temperature SFF can be understood directly from the exact partition function. At $\beta = 0$,

$$Z(-it) = \text{Tr} e^{iHt} = 4^M + \prod_{q=1}^M 4 \cos^2\left(\frac{\epsilon_q t}{2}\right), \quad (\text{C16})$$

where $M = \lfloor (N-1)/2 \rfloor$. Using $Z(0) = 2^N = 2 \cdot 4^M$ for odd N , this can be written as

$$\frac{Z(-it)}{Z(0)} = \frac{1}{2} \left[1 + P_N^2\left(\frac{t}{2}\right) \right], \quad (\text{C17})$$

where

$$P_N(x) = \prod_{q=1}^M \cos(\epsilon_q x). \quad (\text{C18})$$

Therefore

$$g(t, 0) = \frac{1}{4} \left[1 + P_N^2\left(\frac{t}{2}\right) \right]^2. \quad (\text{C19})$$

This form makes the origin of the plateau transparent. The first term in $Z(it)$ comes from the extensive frozen sector and is strictly time independent. The second term comes from the active sector and is controlled by $P_N(x)$. As shown in Appendix C3, $P_N(x)$ is exponentially suppressed at large N for any fixed $x \neq 0$. It follows that for fixed $t > 0$,

$$P_N\left(\frac{t}{2}\right) \rightarrow 0, \quad N \rightarrow \infty, \quad (\text{C20})$$

and Eq. (C19) reduces to

$$g(t, 0) \xrightarrow{N \rightarrow \infty} \frac{1}{4}. \quad (\text{C21})$$

This is the plateau value quoted in Sec. IV B.

3. Large- N estimate of $P_N(x)$

Here we estimate the large- N behavior of $P_N(x)$ defined in Eq. (C18). Following Ref. [26], we introduce the single-particle density of states

$$\begin{aligned} D_1(\epsilon) &= \frac{1}{2M+1} \sum_{q=1}^M \left[\delta(\epsilon - \epsilon_q) + \delta(\epsilon + \epsilon_q) \right] \\ &\simeq \int_{-1/2}^{1/2} dq \delta(\epsilon - \cot(\pi q)) = \frac{1}{\pi} \frac{1}{1 + \epsilon^2}, \end{aligned} \quad (\text{C22})$$

where $M = \lfloor (N-1)/2 \rfloor$.

Replacing the sum over q by an integral, we obtain

$$\log |P_N(x)| \simeq \frac{N}{2\pi} \int_{-\infty}^{\infty} d\epsilon \frac{1}{1 + \epsilon^2} \log |\cos(\epsilon x)|. \quad (\text{C23})$$

Evaluating the integral gives

$$|P_N(x)| \simeq \left(\frac{1 + e^{-2|x|}}{2} \right)^N, \quad (\text{C24})$$

and in the scaling regime with $u = N|x|$ fixed,

$$|P_N(u/N)| = \exp\left[-u + O\left(\frac{1}{N}\right)\right]. \quad (\text{C25})$$

Thus, $P_N(x)$ is exponentially suppressed in both N and $|x|$, which explains the rapid approach to the plateau in Eq. (C19).

Appendix D: Details of dynamics and correlation functions

This Appendix collects the technical steps behind Sec. V. We derive the projector form of the evolution operator, the sector decomposition of the thermal state and its weights, the momentum-space Green functions, and the complex-time representation and Wick reduction of the regularized OTOC.

1. Projector form of time evolution

Using the factorized Hamiltonian in Eq. (16) and the projectors introduced in Eq. (33), we obtain

$$HP_0 = 0, \quad HP_1 = H_{\text{pair}}P_1, \quad (\text{D1})$$

and therefore

$$e^{-iHt} = P_0 + P_1 e^{-iH_{\text{pair}}t}. \quad (\text{D2})$$

For any operator O , this gives

$$\begin{aligned} O(t) &= e^{iHt} O e^{-iHt} \\ &= P_0 O P_0 + P_1 e^{iH_{\text{pair}}t} O e^{-iH_{\text{pair}}t} P_1 + P_0 O P_1 + P_1 O P_0. \end{aligned} \quad (\text{D3})$$

This is the decomposition used in Sec. V.

2. Thermal density matrix, partition functions, and sector weights

Because the Hamiltonian factorizes as in Eq. (16), the Boltzmann weight separates into the two sectors:

$$e^{-\beta H} = P_0 + P_1 e^{-\beta H_{\text{pair}}}. \quad (\text{D4})$$

Taking the trace gives

$$Z = \text{Tr} e^{-\beta H} = \text{Tr}(P_0) + \text{Tr}_{\text{pair}}\left(e^{-\beta H_{\text{pair}}}\right), \quad (\text{D5})$$

where Tr_{pair} denotes the trace over the paired Bogoliubov modes $\{n_{q\sigma}\}$ with $q = 1, \dots, M$ and $\sigma = \pm 1$. For even N , the unpaired $q = N/2$ mode contributes an overall factor 2 independent of β ; we suppress it here since it cancels in normalized quantities.

Using $\text{Tr}(P_0) = 2^{N-1}$ and the diagonal form of H_{pair} , the active-sector contribution becomes

$$\begin{aligned} Z_{\text{pair}} &:= \text{Tr}_{\text{pair}} \left(e^{-\beta H_{\text{pair}}} \right) \\ &= \prod_{q=1}^M \prod_{\sigma=\pm 1} \left(1 + e^{-\beta \sigma \epsilon_q} \right) \\ &= \prod_{q=1}^M \left(2 + 2 \cosh(\beta \epsilon_q) \right) = \prod_{q=1}^M 4 \cosh^2 \left(\frac{\beta \epsilon_q}{2} \right). \end{aligned} \quad (\text{D6})$$

Hence the sector weights introduced in Sec. V are

$$w_1(\beta, N) = \frac{Z_{\text{pair}}}{4^M + Z_{\text{pair}}}, \quad w_0 = 1 - w_1. \quad (\text{D7})$$

The normalized thermal state can then be written as

$$\rho = \frac{e^{-\beta H}}{Z} = w_0 \rho^{(0)} + w_1 \rho^{(1)}. \quad (\text{D8})$$

Here

$$\rho^{(0)} = \frac{P_0}{\text{Tr}(P_0)}, \quad \rho^{(1)} = \frac{P_1 e^{-\beta H_{\text{pair}}}}{Z_{\text{pair}}}. \quad (\text{D9})$$

This gives the decomposition used in Eq. (36). Since both $\rho^{(0)}$ and $\rho^{(1)}$ are Gaussian, Wick's theorem applies separately in the two sectors.

3. Momentum-space correlators and analytic continuation

In the active sector, the state $\rho^{(1)}$ is Gaussian in the Bogoliubov basis. Using Eq. (18), the quasiparticles evolve as

$$\gamma_{q\sigma}(t) = e^{-i\sigma\epsilon_q t} \gamma_{q\sigma}, \quad (\text{D10})$$

and their occupations are

$$\langle n_{q\sigma} \rangle^1 = \frac{1}{1 + e^{\beta\sigma\epsilon_q}} = \frac{1}{2} \left(1 - \sigma \tanh \frac{\beta\epsilon_q}{2} \right). \quad (\text{D11})$$

Using

$$f_q = \frac{1}{\sqrt{2}} (\gamma_{q+} + \gamma_{q-}), \quad f_{N-q}^\dagger = \frac{i}{\sqrt{2}} (\gamma_{q+} - \gamma_{q-}), \quad (\text{D12})$$

one obtains the momentum-space contractions quoted in Eqs. (41) and (42):

$$\langle f_q^\dagger(t) f_q(0) \rangle^1 = \frac{1}{2} \left[\cos(\epsilon_q t) - i \tanh \left(\frac{\beta\epsilon_q}{2} \right) \sin(\epsilon_q t) \right], \quad (\text{D13})$$

$$\langle f_q(t) f_{N-q}(0) \rangle^1 = -\frac{1}{2} \left[\sin(\epsilon_q t) + i \tanh \left(\frac{\beta\epsilon_q}{2} \right) \cos(\epsilon_q t) \right]. \quad (\text{D14})$$

The remaining components follow from Hermitian conjugation and fermionic antisymmetry.

Since these expressions are finite sums of $\sin(\epsilon_q t)$ and $\cos(\epsilon_q t)$, they extend directly to complex time $t \rightarrow t + i\tau$. This is the extension used in the regularized OTOC.

In the frozen sector, the Hamiltonian vanishes and the state is time independent. The projected ensemble is Gaussian on the nonzero-momentum modes, with

$$\langle f_p^\dagger f_{p'} \rangle^0 = \frac{1}{2} \delta_{pp'}, \quad \langle f_p f_{p'} \rangle^0 = 0, \quad (p, p' \neq 0). \quad (\text{D15})$$

Hence all time dependence in the two-point functions comes from the active sector.

4. Real-space correlators at finite N

Using the inverse Fourier transform, we obtain the real-space correlators from the momentum-space expressions in Appendix D 3.

We begin with the anomalous correlator $\langle c_j(t) c_k(0) \rangle$. Substituting the Fourier expansion,

$$\langle c_j(t) c_k(0) \rangle = \frac{1}{N} \sum_{p,q} e^{i\theta_p j} e^{i\theta_q k} \langle f_p(t) f_q(0) \rangle. \quad (\text{D16})$$

Since $\langle f_p(t) f_q(0) \rangle$ is nonzero only when $q = N - p$, we obtain

$$\begin{aligned} \langle c_j(t) c_k(0) \rangle &= \frac{i w_1}{2N} \sum_{q=1}^{\lfloor (N-1)/2 \rfloor} \sin[\theta_q(j-k)] \\ &\quad \times \left[-\sin(\epsilon_q t) - i \tanh \left(\frac{\beta\epsilon_q}{2} \right) \cos(\epsilon_q t) \right]. \end{aligned} \quad (\text{D17})$$

The $q = 0$ mode does not contribute. For even N , the unpaired mode $q = N/2$ also drops out because its anomalous correlator vanishes.

Similarly,

$$\langle c_j^\dagger(t) c_k^\dagger(0) \rangle = -\langle c_j(t) c_k(0) \rangle. \quad (\text{D18})$$

We next consider the correlators involving one creation operator and one annihilation operator. In this case, the $q = 0$ mode contributes explicitly, and for even N the unpaired mode $q = N/2$ gives an additional term of order $1/N$. One finds

$$\begin{aligned} \langle c_j(t) c_k^\dagger(0) \rangle &= \frac{w_0}{2} \delta_{jk} + \frac{w_0}{N} \left[P_N^2 \left(\frac{t}{2} \right) - \frac{1}{2} \right] \\ &\quad + \frac{w_1}{N} \sum_{q=1}^{\lfloor (N-1)/2 \rfloor} \cos[\theta_q(j-k)] \\ &\quad \times \left[\cos(\epsilon_q t) - i \tanh \left(\frac{\beta\epsilon_q}{2} \right) \sin(\epsilon_q t) \right] \\ &\quad + \delta_{N,\text{even}} \frac{w_1}{2N} e^{i\pi(j-k)}, \end{aligned} \quad (\text{D19})$$

and

$$\begin{aligned} \langle c_j^\dagger(t) c_k(0) \rangle &= \frac{w_0}{2} \delta_{jk} - \frac{w_0}{2N} \\ &+ \frac{w_1}{N} \sum_{q=1}^{\lfloor (N-1)/2 \rfloor} \cos[\theta_q(j-k)] \\ &\quad \times \left[\cos(\epsilon_q t) - i \tanh\left(\frac{\beta \epsilon_q}{2}\right) \sin(\epsilon_q t) \right] \\ &+ \frac{w_1}{N} \frac{P_N^2\left(\frac{t+i\beta}{2}\right)}{P_N^2\left(\frac{i\beta}{2}\right)} + \delta_{N,\text{even}} \frac{w_1}{2N} e^{i\pi(j-k)}. \end{aligned} \quad (\text{D20})$$

Here $P_N(x)$ is defined in Eq. (C18). The last term appears only for even N and comes from the unpaired mode $q = N/2$. Thus, at finite N , the difference between these two correlators comes from the $q = 0$ contribution and, for even N , from the unpaired mode $q = N/2$.

5. Complex-time representation and Wick reduction of the regularized OTOC

Starting from the regularized OTOC in Eq. (45), we write $\rho^{1/4} = Z^{-1/4} e^{-\beta H/4}$ and use cyclicity of the trace to absorb the imaginary-time shifts into the operator arguments. This gives

$$\mathcal{F}(t; \beta) = \frac{1}{N^2} \sum_{j,m} \text{Tr} \left[\rho c_j^\dagger(t_1) c_m(t_2) c_j(t_3) c_m(t_4) \right], \quad (\text{D21})$$

evaluated at

$$(t_1, t_2, t_3, t_4) = (t - i\beta/4, 0, t + i\beta/4, i\beta/2). \quad (\text{D22})$$

This is the representation used in Sec. VB.

Using Eq. (D8), the OTOC decomposes as

$$\mathcal{F}(t; \beta) = w_0 \mathcal{F}^0(t; \beta) + w_1 \mathcal{F}^1(t; \beta), \quad (\text{D23})$$

where \mathcal{F}^α denotes the same four-point function evaluated in the Gaussian state $\rho^{(\alpha)}$. In the frozen sector, the Hamiltonian is zero, so \mathcal{F}^0 is time independent. All nontrivial time dependence comes from \mathcal{F}^1 in the active sector.

Within each sector, Wick's theorem applies. Let

$$\begin{aligned} A &= c_j^\dagger(t_1), & B &= c_m(t_2), \\ C &= c_j(t_3), & D &= c_m(t_4). \end{aligned} \quad (\text{D24})$$

Then

$$\langle ABCD \rangle^\alpha = \langle AB \rangle^\alpha \langle CD \rangle^\alpha - \langle AC \rangle^\alpha \langle BD \rangle^\alpha + \langle AD \rangle^\alpha \langle BC \rangle^\alpha. \quad (\text{D25})$$

Therefore,

$$\begin{aligned} \mathcal{F}^\alpha(t; \beta) &= \frac{1}{N^2} \sum_{j,m} \left[\langle c_j^\dagger(t_1) c_m(t_2) \rangle^\alpha \langle c_j(t_3) c_m(t_4) \rangle^\alpha \right. \\ &\quad - \langle c_j^\dagger(t_1) c_j(t_3) \rangle^\alpha \langle c_m(t_2) c_m(t_4) \rangle^\alpha \\ &\quad \left. + \langle c_j^\dagger(t_1) c_m(t_4) \rangle^\alpha \langle c_m(t_2) c_j(t_3) \rangle^\alpha \right], \end{aligned} \quad (\text{D26})$$

with (t_1, t_2, t_3, t_4) given by Eq. (D22). All two-point functions entering Eq. (D26) are obtained from the sector Green functions by analytic continuation to the complex time differences $t_a - t_b$.

6. Large- N limit of the correlators and the OTOC

We now take the large- N limit of the real-space correlators obtained in Appendix D4. The contributions from the $q = 0$ mode and, for even N , from the unpaired mode $q = N/2$ are all of order $1/N$, and therefore vanish in the large N limit. By contrast, the sums over the paired modes remain finite and are replaced by integrals over $\theta \in [0, \pi]$, with $\epsilon(\theta) = \cot(\frac{\theta}{2})$. Applying this to Eq. (D17), we obtain

$$\begin{aligned} \langle c_j(t) c_k(0) \rangle &\xrightarrow{N \rightarrow \infty} i \frac{w_1}{2\pi} \int_0^\pi d\theta \sin[\theta(j-k)] \\ &\quad \times \left[-\sin(\epsilon(\theta)t) - i \tanh\left(\frac{\beta \epsilon(\theta)}{2}\right) \cos(\epsilon(\theta)t) \right]. \end{aligned} \quad (\text{D27})$$

Equation (D18) continues to hold in the large- N limit.

Similarly, Eqs. (D19) and (D20) reduce to

$$\begin{aligned} \langle c_j(t) c_k^\dagger(0) \rangle &= \langle c_j^\dagger(t) c_k(0) \rangle + O(N^{-1}) \\ &\xrightarrow{N \rightarrow \infty} \frac{w_0}{2} \delta_{jk} + \frac{w_1}{2\pi} \int_0^\pi d\theta \cos[\theta(j-k)] \\ &\quad \times \left[\cos(\epsilon(\theta)t) - i \tanh\left(\frac{\beta \epsilon(\theta)}{2}\right) \sin(\epsilon(\theta)t) \right]. \end{aligned} \quad (\text{D28})$$

Thus, although the two mixed correlators differ at finite N , they become equal in the large- N limit.

For the OTOC, it is convenient to introduce the Fourier kernels of the large- N Green functions through

$$(G_{XY}^\alpha)_{jk}(t) = \int_{-\pi}^\pi \frac{d\theta}{2\pi} e^{i\theta(j-k)} \mathcal{G}_{XY}^\alpha(\theta; t). \quad (\text{D29})$$

From Eqs. (D27) and (D28), one obtains

$$\mathcal{G}_{cc}^1(\theta; t) = \frac{1}{2i} \left[\tanh\left(\frac{\beta \epsilon(\theta)}{2}\right) \cos(\epsilon(\theta)t) - i \sin(\epsilon(\theta)t) \right], \quad (\text{D30})$$

$$\mathcal{G}_{c^\dagger c}^1(\theta; t) = \frac{1}{2} \left[\cos(\epsilon(\theta)t) - i \tanh\left(\frac{\beta \epsilon(\theta)}{2}\right) \sin(\epsilon(\theta)t) \right], \quad (\text{D31})$$

while

$$\mathcal{G}_{cc}^0(\theta; t) = 0, \quad \mathcal{G}_{c^\dagger c}^0(\theta; t) = \frac{1}{2}. \quad (\text{D32})$$

The remaining components follow from Eq. (D18) and Eq. (D28).

Substituting Eq. (D29) into Eq. (D26), the sums over j and m are converted into momentum integrals by orthogonality.

The sector-resolved OTOC therefore becomes

$$\begin{aligned} \mathcal{F}^\alpha(t; \beta) &= \int_{-\pi}^{\pi} \frac{d\theta}{2\pi} \mathcal{G}_{c^\dagger c}^\alpha(\theta; t_{12}) \mathcal{G}_{cc}^\alpha(-\theta; t_{34}) \\ &\quad - \left[\int_{-\pi}^{\pi} \frac{d\theta}{2\pi} \mathcal{G}_{c^\dagger c}^\alpha(\theta; t_{13}) \right] \left[\int_{-\pi}^{\pi} \frac{d\theta}{2\pi} \mathcal{G}_{cc}^\alpha(\theta; t_{24}) \right] \\ &\quad + \int_{-\pi}^{\pi} \frac{d\theta}{2\pi} \mathcal{G}_{c^\dagger c}^\alpha(\theta; t_{14}) \mathcal{G}_{cc}^\alpha(-\theta; t_{23}), \end{aligned} \quad (\text{D33})$$

where (t_1, t_2, t_3, t_4) is given by Eq. (D22). The full OTOC then follows from Eq. (D23).

The large- N representation above underlies both the plateau behavior described in Sec. VB and the early-time fit used in Sec. VC.

Appendix E: Disorder-free one-dimensional breakdown interaction

In this appendix, we briefly explain how a related sector picture appears in a disorder-free one-dimensional breakdown interaction. The point is that, after removing disorder and performing the same on-site Fourier transform as in the main text, the intersite interaction necessarily involves a distinguished symmetric mode on each site. This gives a simple interpretation of the resulting Hilbert-space fragmentation and the associated spectral degeneracies.

We start from the original breakdown interaction [13],

$$H_I = \sum_{m=1}^{M-1} \sum_{1 \leq i < j < k \leq N} \sum_{l=1}^N \left(J_{m,l}^{ijk} c_{m+1,i}^\dagger c_{m+1,j}^\dagger c_{m+1,k}^\dagger c_{m,l} + \text{H.c.} \right), \quad (\text{E1})$$

where $m = 1, \dots, M$ labels the site along the chain, and $i, j, k, l = 1, \dots, N$ label the internal fermion modes within each site.

To define a disorder-free version, we choose a uniform coupling,

$$J_{m,l}^{ijk} \equiv J. \quad (\text{E2})$$

Then Eq. (E1) becomes

$$H_I^{(\text{df})} = J \sum_{m=1}^{M-1} \sum_{1 \leq i < j < k \leq N} \sum_{l=1}^N \left(c_{m+1,i}^\dagger c_{m+1,j}^\dagger c_{m+1,k}^\dagger c_{m,l} + \text{H.c.} \right). \quad (\text{E3})$$

Next we perform the same Fourier transform on each site,

$$f_p^{(m)} \equiv \frac{1}{\sqrt{N}} \sum_{\ell=1}^N c_{m,\ell} e^{-i\frac{2\pi}{N} p \ell}, \quad p = 0, 1, \dots, N-1, \quad (\text{E4})$$

so that the symmetric mode is

$$f_0^{(m)} = \frac{1}{\sqrt{N}} \sum_{\ell=1}^N c_{m,\ell}, \quad \sum_{\ell=1}^N c_{m,\ell} = \sqrt{N} f_0^{(m)}. \quad (\text{E5})$$

Introducing

$$A^{(m+1)} \equiv \sum_{1 \leq j < k \leq N} c_{m+1,j}^\dagger c_{m+1,k}^\dagger, \quad (\text{E6})$$

we obtain

$$H_I^{(\text{df})} = NJ \sum_{m=1}^{M-1} \left(f_0^{\dagger(m+1)} f_0^{(m)} A^{(m+1)} + A^{\dagger(m+1)} f_0^{\dagger(m)} f_0^{(m+1)} \right), \quad (\text{E7})$$

which has the same basic structure as the factorized form in Eq. (16), except that the distinguished modes now live on neighboring sites.

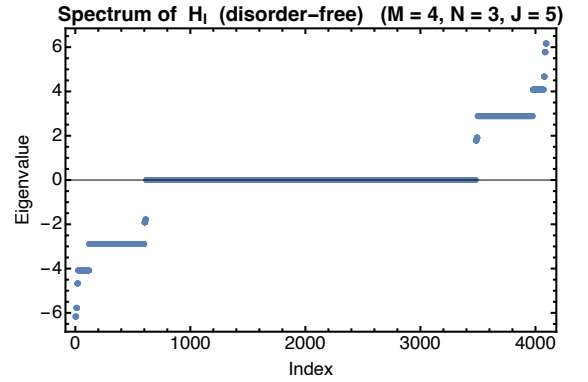


FIG. 11. Eigenvalues of the disorder-free one-dimensional breakdown interaction $H_I^{(\text{df})}$, sorted in ascending order. The parameters are $M = 4$ sites, $N = 3$ modes per site, and coupling $J = 5$.

Defining the site-resolved occupation

$$n_0^{(m)} \equiv f_0^{\dagger(m)} f_0^{(m)}, \quad (\text{E8})$$

we see from Eq. (E7) that any intersite breakdown process necessarily involves the symmetric mode on the corresponding site. In particular, if $n_0^{(m)} = 0$ on a given many-body basis state, then the forward process from site m to $m+1$ is blocked, because the annihilation operator $f_0^{(m)}$ acts trivially on that state. As an extreme example, the subspace with $n_0^{(m)} = 0$ for all m is annihilated by $H_I^{(\text{df})}$, giving a large family of exact eigenstates and hence extensive degeneracies. More generally, the dynamics generated by $H_I^{(\text{df})}$ is strongly constrained by the pattern $\{n_0^{(m)}\}$, which provides a natural origin of the fragmentation structure in this disorder-free one-dimensional model; see Fig. 11.

Finally, in the original $N = 3$ model, the special mode $f_{m,1}$ is defined by an on-site $U(3)$ rotation [13]. In the uniform-coupling disorder-free case, symmetry allows one to choose $f_{m,1}$ as the symmetric combination, that is, $f_{m,1} \equiv f_0^{(m)}$ up to a phase, whereas this identification does not hold for generic couplings.

- [1] J. Townsend, *The theory of ionization of gases by collision* (Constable, Limited, 1910).
- [2] S. M. Sze and G. Gibbons, Avalanche breakdown voltages of abrupt and linearly graded p–n junctions in Ge, Si, GaAs, and GaP, in *Semiconductor Devices: Pioneering Papers* (World Scientific, 1991) pp. 141–143.
- [3] A. Sun, C. Huo, and J. Zhuang, Formation mechanism of streamer discharges in liquids: a review, *High Voltage* **1**, 74 (2016).
- [4] S. Yamanouchi, Y. Taguchi, and Y. Tokura, Dielectric Breakdown of the Insulating Charge-Ordered State in $\text{La}_{2-x}\text{Sr}_x\text{NiO}_4$, *Phys. Rev. Lett.* **83**, 5555 (1999).
- [5] Y. Taguchi, T. Matsumoto, and Y. Tokura, Dielectric breakdown of one-dimensional Mott insulators Sr_2CuO_3 and SrCuO_2 , *Phys. Rev. B* **62**, 7015 (2000).
- [6] H. Akiyama, Streamer discharges in liquids and their applications, *IEEE Transactions on dielectrics and electrical Insulation* **7**, 646 (2000).
- [7] J. R. Claycomb, K. E. Bassler, J. Miller, J. H., M. Nersisyan, and D. Luss, Avalanche behavior in the dynamics of chemical reactions, *Physical Review Letters* **87**, 178303 (2001).
- [8] Y. P. Raizer, J. E. Allen, *et al.*, *Gas discharge physics* (Springer, 1991).
- [9] M. A. Lieberman and A. J. Lichtenberg, *Principles of Plasma Discharges and Materials Processing* (John Wiley & Sons, 2005).
- [10] T. Fukui and N. Kawakami, Breakdown of the mott insulator: Exact solution of an asymmetric hubbard model, *Physical Review B* **58**, 16051 (1998).
- [11] T. Oka and H. Aoki, Dielectric breakdown in a mott insulator: Many-body schwinger-landau-zener mechanism studied with a generalized bethe ansatz, *Physical Review B* **81**, 033103 (2010).
- [12] T. Oka and H. Aoki, Nonequilibrium quantum breakdown in a strongly correlated electron system, in *Quantum and Semi-classical Percolation and Breakdown in Disordered Solids*, Lecture Notes in Physics, Vol. 762, edited by A. K. Sen, K. K. Bardhan, and B. K. Chakrabarti (Springer, 2008) pp. 251–286.
- [13] B. Lian, Quantum breakdown model: From many-body localization to chaos with scars, *Physical Review B* **107**, 115171 (2023).
- [14] B.-T. Chen, A. Prem, N. Regnault, and B. Lian, Quantum fragmentation in the extended quantum breakdown model, *Physical Review B* **110**, 165109 (2024).
- [15] Y.-M. Hu and B. Lian, From the quantum breakdown model to the lattice gauge theory, *AAPPS Bulletin* **34**, 24 (2024).
- [16] X. Liu and B. Lian, Two-dimensional quantum breakdown model with krylov subspace many-body localization, *Physical Review B* **111**, 054302 (2025).
- [17] Y.-M. Hu, Z. Han, and B. Lian, Quantum breakdown condensate as a disorder-free quantum glass, arXiv preprint arXiv:2512.21847 (2025).
- [18] S. Sachdev and J. Ye, Gapless spin-fluid ground state in a random quantum heisenberg magnet, *Physical Review Letters* **70**, 3339 (1993).
- [19] A. Kitaev, A simple model of quantum holography (part 1), talk at KITP, April 7, 2015 (2015).
- [20] O. Bohigas, M.-J. Giannoni, and C. Schmit, Characterization of chaotic quantum spectra and universality of level fluctuation laws, *Physical Review Letters* **52**, 1 (1984).
- [21] J. S. Cotler, G. Gur-Ari, M. Hanada, J. Polchinski, P. Saad, S. H. Shenker, D. Stanford, A. Streicher, and M. Tezuka, Black holes and random matrices, *Journal of High Energy Physics* **2017**, 118 (2017).
- [22] A. I. Larkin and Y. N. Ovchinnikov, Quasiclassical method in the theory of superconductivity, *Sov Phys JETP* **28**, 1200 (1969).
- [23] J. Maldacena, S. H. Shenker, and D. Stanford, A bound on chaos, *Journal of High Energy Physics* **2016**, 106 (2016).
- [24] J. Maldacena and D. Stanford, Remarks on the Sachdev–Ye–Kitaev model, *Physical Review D* **94**, 106002 (2016).
- [25] P. Hosur, X.-L. Qi, D. A. Roberts, and B. Yoshida, Chaos in quantum channels, *Journal of High Energy Physics* **2016**, 1 (2016).
- [26] S. Ozaki and H. Katsura, Disorder-free Sachdev–Ye–Kitaev models: Integrability and a precursor of chaos, *Physical Review Research* **7**, 013092 (2025).
- [27] E. Iyoda, H. Katsura, and T. Sagawa, Effective dimension, level statistics, and integrability of Sachdev–Ye–Kitaev-like models, *Phys. Rev. D* **98**, 086020 (2018).
- [28] Nivedita, L. Shackleton, and S. Sachdev, Spectral form factors of clean and random quantum ising chains, *Physical Review E* **101**, 042136 (2020).
- [29] A. Campa, T. Dauxois, and S. Ruffo, Statistical mechanics and dynamics of solvable models with long-range interactions, *Physics Reports* **480**, 57 (2009).
- [30] N. Defenu, T. Donner, T. Macrì, G. Pagano, S. Ruffo, and A. Trombettoni, Long-range interacting quantum systems, *Reviews of Modern Physics* **95**, 035002 (2023).
- [31] J. L. Cardy, Conformal invariance and universality in finite-size scaling, *Journal of Physics A: Mathematical and General* **17**, L385 (1984).
- [32] H. W. J. Blöte, J. L. Cardy, and M. P. Nightingale, Conformal invariance, the central charge, and universal finite-size amplitudes at criticality, *Physical Review Letters* **56**, 742 (1986).
- [33] I. Affleck, Universal term in the free energy at a critical point and the conformal anomaly, *Physical Review Letters* **56**, 746 (1986).
- [34] H. Afshar, H. A. González, D. Grumiller, and D. Vassilevich, Flat space holography and the complex Sachdev–Ye–Kitaev model, *Physical Review D* **101**, 086024 (2020).